Applied Catalysis B: Environmental 163 (2015) 267–276

Contents lists available at ScienceDirect

Applied Catalysis B: Environmental

journal homepage: www.elsevier.com/locate/apcatb

Efficient organic degradation under visible light by α-Bi_2O_3 with a CuO_x-assistant electron transfer process

Hai-Ying Jiang[a,b], Guigao Liu[a], Mu Li[a], Jingjing Liu[b], Wenbin Sun[b], Jinhua Ye[a,*], Jun Lin[b,*]

[a] International Center for Materials Nanoarchitectonics (WPI-MANA), and Enviromental Remediation Materials Unit, National Institute for Materials Science (NIMS), 1-1, Namiki, Tsukuba, Ibaraki 305-0044, Japan
[b] Department of Chemistry, Renmin University of China, Beijing 100872, People's Republic of China

ARTICLE INFO

Article history:
Received 17 February 2014
Received in revised form 11 July 2014
Accepted 26 July 2014
Available online 4 August 2014

Keywords:
Photocatalyst
α-Bi_2O_3
CuO_x modification
CuO_x-assistance electron transfer process (CuO_x-AETP)
Cu cycle

ABSTRACT

In this study, we have found that CuO_x modified α-Bi_2O_3 is an excellent photocatalytic material for the visible-light-driven degradation of various organic compounds including RhB, MO, 2,4-DCP, and gaseous IPA. A detailed study on the mechanism of the photocatalytic reaction was performed by measuring the photogenerated •OH and H_2O_2 under visible light irradiation. The results indicate that modifying CuO_x on the surface of α-Bi_2O_3 significantly promotes the separation of the photogenerated electrons and holes of α-Bi_2O_3. The important role of CuO_x was further investigated by detecting the valence states change of Cu before and after the photocatalysis, using ESR and XPS. It was found that, the Cu states within the CuO_x clusters are the coexistence of Cu(II) clusters, CuO and Cu. As a result, the enhancement of photocatalytic activity by CuO_x modification can be attributed to a CuO_x-assistant electron transfer process (CuO_x-AETP), which involves in two electron excitation paths and a Cu cycle of different valence states.

1. Introduction

Environmental pollution by organic pollutants is becoming an increasingly serious problem due to industrialization and an increase in population. Photocatalysis, a relatively new cross-disciplinary field, began with the discovery of the photocatalytic splitting of water molecules on TiO_2 electrode in 1972 [1]. TiO_2 [2–5], as the most effective known photocatalyst, has been widely used as an environment cleaning material. The key process of the efficient photocatalytic reactions is the effective separation of the photogenerated carriers produced by band-gap excitation under the light irradiation. The carriers usually have favorable oxidation or reduction electrical potentials to trap O_2, H_2O, and OH^- on the surface of the semiconductors, forming highly active radicals, such as O_2^{-}•, •OH and •HO_2 [6]. All three radicals are very strong oxidizing species and act as initiators for contaminant mineralization. Scientists have developed and studied a series of semiconductors, e.g. TiO_2 [2–5], ZnO [7–9], etc., as the photocatalysts for driving the chemical degradation and mineralization of organic contaminants under visible light irradiation. However, since the traditional photocatalysts can be only excited upon UV irradiation due to their relatively wide band gaps, their application in our daily life are hindered. As a result, narrow band gap semiconductors, e.g. WO_3 [10,11], Bi_2WO_6 [12,13], Bi_2O_3 [14–19], etc., are increasingly becoming more attractive as the potential photocatalysts in the recent years, because of their visible light response.

α-Bi_2O_3, a fascinating material widely used for the solid oxide fuel cells, fire retardants, functional ceramic materials, optical coatings and devices, superconductors, and gas sensors [20–23], has been proved to be a promising visible-light-responsive photocatalyst with respects to its unique properties, such as relatively narrow band gap (~2.8 eV), deep valence band (~+3.13 V vs. NHE), environmentally friendship (nontoxic, low-radioactivity) as TiO_2 [24], and thermal stability [25]. There has also been much research on the hierarchical nanostructures [19], nanotubes [18,26], nanofibers [27] and other morphemic modified α-Bi_2O_3 [15]. In these studies, α-Bi_2O_3 has shown definite photocatalytic activity and is believed to be a potential and meaningful photocatalyst for the practical applications. Therefore, much recent research has been focused on developing useful strategies to improve the photocatalytic activity of α-Bi_2O_3. There have been some researches being reported, which mainly include the morphologies [15,19,26,27], surface modifications [16,17,20], heterojunction constructions [28,29] and heteroatom dopings [17].

In previous studies, Cu(II) clusters and CuO modifications have been widely used as effective strategies to improve the photocatalytic activities of some semiconductors, such as TiO_2 [30–33], WO_3 [31,34] and $(Sr_{1-y}Na_y)(Ti_{1-x}Mo_x)O_3$ [35]. Cu(II) clusters and CuO

* Corresponding authors. Tel.: +81 29 859 2646; fax: +81 29 860 4958.
E-mail address: Jinhua.YE@nims.go.jp (J. Ye).

http://dx.doi.org/10.1016/j.apcatb.2014.07.058
0926-3373/

are considered as good co-catalysts because they are noble metal free, which is consistent with the low-cost request in nowadays. In order to develop α-Bi_2O_3 as an efficient visible-light responsive photocatalyst, we prepared the CuO_x modified α-Bi_2O_3 samples with a simple impregnation method. In this paper, the photocatalytic activity of α-Bi_2O_3, in degradation of different dye and non-dye contaminants under visible light irradiation, has been widely and significantly enhanced by CuO_x modification. The phase structures and optical absorptions of the samples were studied by the XRD and UV–vis DRS; the morphologies and microstructures were observed by SEM, TEM and HRTEM; the chemical states of the elements within all samples were analyzed by XPS. Based on the experimental results, we concluded that the states of the Cu are the coexistence of Cu(II) clusters, CuO and Cu. Furthermore, we also studied the role of the CuO_x by monitoring the photocatalytic generations of $^{\bullet}OH$ and H_2O_2 over α-Bi_2O_3 and CuO_x/α-Bi_2O_3 samples. The photocatalytic mechanism of CuO_x/α-Bi_2O_3 was also studied by the ESR and XPS measurements of Cu(II) species. In this work, the CuO_x-assistant electron transfer process (CuO_x-AETP) was proposed, which involves in two electron excitation paths and a Cu cycle of different valence states.

2. Experimental

2.1. Sample preparations

All chemical reagents of analytical grade were used without further purification as received. The α-Bi_2O_3 sample was prepared from $Bi(NO_3)_3{\cdot}5H_2O$ by hydrolysis under basic conditions [15]. In a typical synthesis, an amount of 10.78 g of Bi $(NO_3)_3{\cdot}5H_2O$ was dissolved in a 30 ml aqueous solution of HNO_3 (1.5 M) to avoid the hydrolyzation of Bi^{3+} ions. Under vigorous agitation, the NaOH solution (50% w/v) was added into the solution dropwise until pH > 13. In that process, yellow precipitate was formed. Subsequently, the suspension was heated to 80 °C and kept for 2 h, and then the precipitate was collected by centrifugation and being washed with deionized water several times. After that, the resultant solid was dried at 120 °C overnight in air. At the end, the powder was calcined at 450 °C for 5 h. CuO_x modified α-Bi_2O_3 samples were prepared with an impregnation method as described in the previous work [30], using $CuCl_2{\cdot}2H_2O$ as Cu source. More specifically, 1 g α-Bi_2O_3 and the designated amounts of $CuCl_2{\cdot}2H_2O$ were dispersed in 10 ml deionized water. The weight ratios of Cu relative to α-Bi_2O_3 were set to be 0.2%, 0.4%, 0.6%, and 0.8%. Under magnetic stirring, the suspension was heated to 90 °C and kept for 1 h in a water bath. Then the suspension was filtered and washed with deionized water several times before being dried at 110 °C for 24 h. Meanwhile, pure α-Bi_2O_3 without CuO_x modification was treated in the same manner.

2.2. Characterization

The crystal structures of pure α-Bi_2O_3 and CuO_x/α-Bi_2O_3 samples were characterized with an X-ray diffractometer (Shimadzu, XRD-7000) with Cu-Kα as X-ray radiation (λ = 0.15418 nm), under 40 kV and 30 mA. The scanning of 2θ was from 20° to 80° at a step of 2θ = 0.02°, 0.5 s/step. The optical absorption spectra of the samples were obtained by UV–vis (Hitachi U-3900) spectrophotometer equipped with a diffuse reflectance accessory, with $BaSO_4$ as the reflectance standard reference. The surface morphologies of the samples were observed by field emission scanning electron microscope (FESEM, JEOL S-4800), while the microstructures of the samples were characterized by a high-resolution transmission electron microscopy (HRTEM, JEOL JEM-2010). The surface areas of the samples were measured by a Brunauer–Emmett–Teller (BET) method through nitrogen adsorption and desorption isotherms at 77 K, using a surface area analyzer (BEL Sorp-mini II, BEL Japan Co., Japan). The surface element compositions and their chemical states in all the samples were analyzed by an X-ray photoelectron spectroscopy (XPS, ESCALab220i-XL), using 300 W Al Kα radiation. All binding energies were referenced with respect to the C 1s peak (284.6 eV) of the surface adventitious carbon.

2.3. Photocatalytic activity measurement

The photocatalytic activities of the pure α-Bi_2O_3 and CuO_x/α-Bi_2O_3 samples were evaluated by the degradation of different dyes [Rhodamine B (RhB), Methyl Orange (MO)] and non-dye organic compounds [2,4-dichlorophenol (2,4-DCP), gaseous 2-propanol (IPA)], in aqueous or gas solutions.

For the RhB ($\sim 1 \times 10^{-5}$ M) and MO ($\sim 4 \times 10^{-5}$ M) aqueous solution degradation, a 300 W Xe arc lamp (CHF-XM150, Beijing Trusttech. Co., Ltd.) equipped with a wavelength cutoff filter ($\lambda \leq 420$ nm) was used as the light source to trigger the photocatalytic reactions over pure α-Bi_2O_3 and CuO_x/α-Bi_2O_3 samples. Typically, the experiments were performed in a beaker with 100 ml aqueous solution of either RhB or MO and 100 mg photocatalyst powder. Before irradiation, the suspensions were continuously stirred in the dark for 1 h so as to achieve the adsorption–desorption equilibrium between the photocatalysts and the RhB or MO molecules. At the given time of 30 min interval, 3 ml of the suspension was sampled. The RhB or MO aqueous solution was separated from the photocatalysts by centrifugation. The concentration changes of RhB and MO were monitored by measuring the absorbance at λ = 554 nm and λ = 461 nm with a UV–vis spectrophotometer (Hitachi U-3310). Meanwhile, the photocatalytic degradation experiments of RhB aqueous solution over CuO_x/α-Bi_2O_3 samples with different weight ratios of Cu were also carried out to determine the optimum Cu weight ratio to α-Bi_2O_3.

In order to avoid the self-sensitized degradation of RhB, the light source was replaced by four 3 W monochromatic lights (λ = 420 nm) to degrade RhB aqueous solutions over pure α-Bi_2O_3 and CuO_x/α-Bi_2O_3 samples. This is because RhB has no absorbance at the wavelength of 420 nm. In addition, to give a further confirmation, the photocatalytic degradation experiments of 2,4-DCP ($\sim 1 \times 10^{-4}$ M), a non-dye organic compound, were also performed in the same conditions. The light source was a 300 W Xe arc lamp (CHF-XM150, Beijing Trusttech. Co., Ltd.) equipped with a wavelength cutoff filter of $\lambda \leq 420$ nm. The light was positioned about 8 cm above the aqueous solution. The degradation of 2,4-DCP was followed by a chromatographic analysis using a high-performance liquid chromatography (DIONEX) with a C18 column. The eluent consists of 65% acetonitrile, 35% water and 0.1% phosphoric acid. The total organic carbon (TOC) of the solutions was also measured using Apollo 9000 apparatus.

The photocatalytic degradation of gaseous IPA was also carried out to verify the improved photocatalytic activity of α-Bi_2O_3 by CuO_x modification. The degradation experiments of IPA were carried out under the visible light with the wavelength of $420\text{ nm} \leq \lambda \leq 800$ nm. The light source was a 300 W Xe-arc lamp (10 A imported current, focused through a 50 mm × 50 mm shutter window), equipped with some wavelength cutoff filters and a water filter. Typically, 200 mg photocatalyst was bespread uniformly on a glass dish with an area of 9 cm^2. A certain amount of gaseous IPA was injected into the vessel and kept for 2 h in the dark before irradiation. During the irradiation by visible light, 0.5 ml of the gas was sampled everyone 1 h intervals. The resultant samples were analyzed using a gas chromatograph (GC-2014, Shimadzu, Japan) with a flame ionization detector (FID). Furthermore, we also carried out the same experiment under the visible light irradiation with the wavelength of $520\text{ nm} < \lambda < 800$ nm, in order to rule out

the singlehanded effect of CuO_x. For comparison, the adsorption experiments of IPA over pure α-Bi_2O_3 and CuO_x/α-Bi_2O_3 samples without light irradiation were also carried out, as well as the self-degradation of IPA without any catalysts under visible light irradiation (420 nm < λ < 800 nm).

2.4. Study of the photocatalytic mechanisms

2.4.1. Analysis of photogenerated •OH

The photocatalytic generation of •OH over pure α-Bi_2O_3 and CuO_x/α-Bi_2O_3 samples was measured in the presence of Fe^{3+} by a fluorescence method using coumarin as a chemical trap (Eq. (1)) [36]. The photocatalysts were dispersed in a 30 ml aqueous solution of 1 mM $FeCl_3$ and 1 mM coumarin, and stirred for 30 min in the dark before being exposed to visible light irradiation (λ ≥ 420 nm). 3 ml suspension was sampled and separated by centrifugation at a given irradiation time interval (10 min). The fluorescence emission intensity evolution of 7-hydroxycoumarin (7-HC), a highly fluorescent product formed from the coumarin and •OH, was detected at about 500 nm under the excitation at 350 nm using a spectrofluorometer (PerkinElmer LS55).

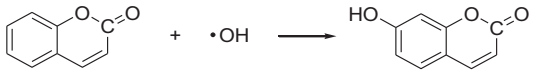

(Coumarin) (7-hydroxycoumarin) (1)

2.4.2. Analysis of photogenerated H_2O_2

The in situ photogeneration of H_2O_2 under visible light irradiation (λ ≥ 420 nm) by the samples were analyzed by using the colorimetric DPD method [37], with methanol as an electron donor. The DPD method was employed because the DPD (N,N-diethyl-p-phenylenediamine) reagents can be easily oxidized by H_2O_2 with the catalysis of POD (horseradish peroxidase).

DPD solution: 0.1 g N,N-diethyl-1,4-phenylenediammonium sulfate (DPD) was dissolved in 10 ml 0.05 M H_2SO_4 to get the DPD solution. POD solution: 10 mg peroxidase (POD) horseradish was dissolved in 10 ml deionized water to get the POD solution. *Buffer*: 0.2 M Na_2HPO_4 solution and 0.2 M NaH_2PO_4 solution were mixed together with the volume ratio of ~1:9 to prepare the phosphate buffer with a pH of 6.0.

60 mg of the photocatalyst was suspended in an aqueous solution composed of 27 ml deionized water, 3 ml phosphate buffer, 50 μL DPD solution, 50 μL POD solution, and 12 μL methanol. The suspension was irradiated by the visible light (λ ≥ 420 nm) after being stirred for 10 min in dark. 3 ml suspension was sampled at a given interval, and monitored by the UV–vis spectrophotometer (Hitachi U-3310) at the wavelength of 551 nm. The concentration of H_2O_2 was determined by a series of standard solutions.

2.4.3. ESR experiment

The electron spin resonance (ESR) measurements were employed to test the valence states change of Cu. The CuO_x/α-Bi_2O_3 sample was dispersed in methanol, and the methanol suspension was bubbled with Ar gas for several minutes to remove the soluble oxygen before being placed into a quartz sample tube. The measurements were performed at 77 K by a JEOL JES-FA 200 ESR spectrometer, with a 500 W Xe lamp as the irradiation source (λ ≥ 420 nm). The Cu(II) spin signals were detected before and after 10 min visible light irradiation. The experimental conditions of the ESR measurements were the center field of 327.813 mT, the sweep width of 5 mT, the microwave frequency of 9167.687 MHz and the microwave power of 2.00 mW.

3. Results and discussion

3.1. Characterizations

3.1.1. Phase structures and optical absorption

The crystal structures of α-Bi_2O_3 and CuO_x/α-Bi_2O_3 samples with different Cu weight ratios were characterized by XRD. Fig. 1 shows the XRD diffraction patterns of the samples, and all the diffraction peaks exhibit a single monoclinic phase of good crystals. The crystal structures of both α-Bi_2O_3 and CuO_x/α-Bi_2O_3 are in accordance with the JCPDS file (No. 41-1449) with the following cell parameters: $a = 5.830$, $b = 8.140$, $c = 7.480$, $\alpha = \gamma = 90°$, $\beta = 67.070°$. As reported [38], among all the six polymorphic forms of bismuth oxide (Bi_2O_3), α phase is the most stable phase at room temperature; δ phase is stable at a high temperature (730–825 °C); the other four phases, i.e. β, γ, ε, and ω, are high temperature metastable. Moreover, we further compared each corresponding diffraction peak of pure α-Bi_2O_3 and CuO_x/α-Bi_2O_3 samples with different Cu weight ratios, and found that they have almost the identical diffraction patterns. No new peaks emerged in any of the CuO_x/α-Bi_2O_3 samples. These results may be because of the over low amounts of the CuO_x on the surface of α-Bi_2O_3. The optical absorbance spectra of all the samples obtained by UV–vis method clearly demonstrate the existence of CuO_x on the surfaces of α-Bi_2O_3. As illustrated in Fig. 2, there is a strong absorption from about 450 nm for pure α-Bi_2O_3 sample, and it results from the intrinsic band gap of α-Bi_2O_3. Differently, two new absorption bands in the range of 450–520 nm and 600–800 nm were observed in the spectra of CuO_x/α-Bi_2O_3 samples with different Cu weight

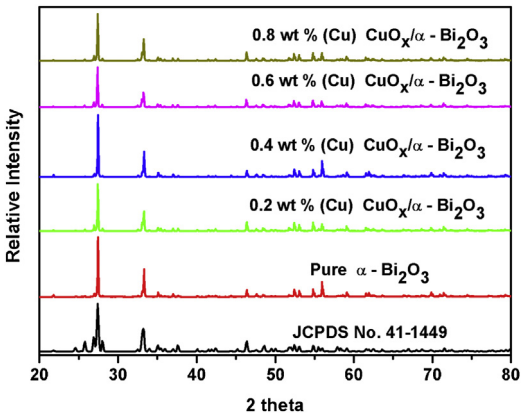

Fig. 1. X-ray diffraction patterns of pure α-Bi_2O_3 and CuO_x/α-Bi_2O_3 with different Cu weight ratios.

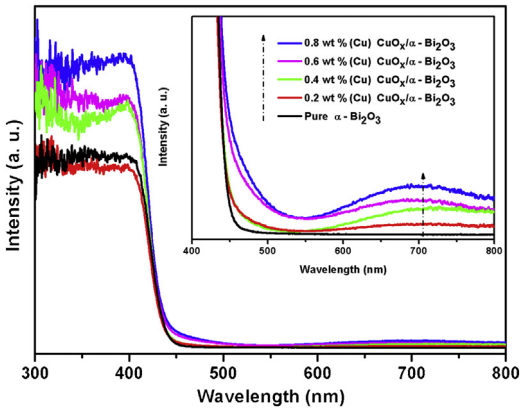

Fig. 2. UV–vis diffuse reflectance spectra of pure α-Bi_2O_3 and CuO_x/α-Bi_2O_3 with different Cu weight ratios.

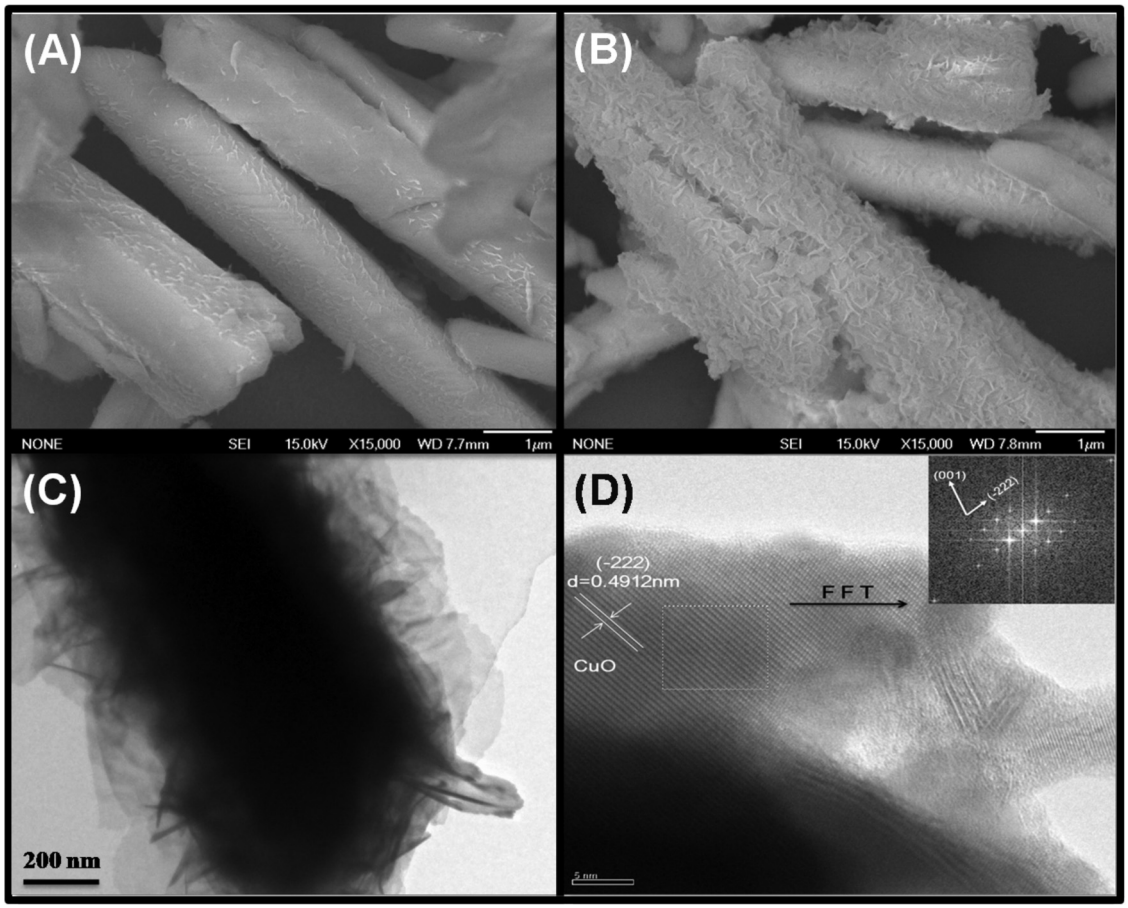

Fig. 3. SEM image of (A) pure α-Bi_2O_3; (B) CuO_x/α-Bi_2O_3; (C) TEM image of CuO_x/α-Bi_2O_3; (D) HRTEM image of CuO_x/α-Bi_2O_3. CuO particle has been expanded and transferred to FFT in the insert for clarifying.

ratios, and they show a gradually increase with the Cu weight ratios increase from 0.2 to 0.8 wt%. According to previous reports [20], the absorption approximately from 450 nm to 520 nm is attributed to the direct interfacial charge transfer (IFCT); the wide range absorption from 600 nm to 800 nm is caused by the d–d transitions of Cu(II). Based on the observations, the existence of Cu(II) clusters on the surface of α-Bi_2O_3can be inferred.

3.1.2. Morphologies

In order to study the morphologies and microstructures of pure α-Bi_2O_3 and CuO_x/α-Bi_2O_3, SEM, TEM and HRTEM were used to observe the samples. The SEM images of pure α-Bi_2O_3 and CuO_x/α-Bi_2O_3 were exhibited in Fig. 3(A) and (B), respectively. In the SEM images, α-Bi_2O_3 is composed of numerous microrods with the dozens of micrometers length and the diameters of 1–2 μm. This result is very similar to the α-Bi_2O_3 prepared by other methods in the earlier literature [39]. Obviously, different morphology of CuO_x/α-Bi_2O_3 can be clearly observed in Fig. 3(B). Based on the rough surface of α-Bi_2O_3 microrods, countless nanosheets have grown and attached to the microrods. From the TEM image in Fig. 3(C), α-Bi_2O_3 microrods are well surrounded by the gauzy nanosheets. Fig. 3(A)–(C) demonstrates the good dispersion of CuO_x on the surface of α-Bi_2O_3. Because the slight wrinkles exist on the surface of α-Bi_2O_3 microrods after CuO_x modification, the increase of the surface area was speculated to occur. The speculation was proved by the BET measurements. The BET surface areas of pure α-Bi_2O_3 and CuO_x/α-Bi_2O_3 are 0.3 m^2/g and 4.1 m^2/g, respectively. Further increasing the magnification, good single-crystalline structure is clearly observed from the image by HRTEM [Fig. 3(D)]. Learn from the previous reports [40], this good single-crystals are most probably the monoclinic CuO crystals. The lattice fringe of 0.4912 nm well matches the (−2 2 2) planes of monoclinic CuO crystals. With a further process of FFT treatment, the other lattice plane is determined to be the (0 0 1) planes of CuO with the lattice fringe of 0.3084 nm [41]. So, the images in Fig. 3 powerfully demonstrate the good deposition and dispersion of CuO on the surface of α-Bi_2O_3 microrods.

3.1.3. XPS spectra analysis

To get more chemical states information of the elements in both α-Bi_2O_3 and CuO_x/α-Bi_2O_3 samples, XPS spectra of every element were also analyzed. The results are presented in Fig. 4(a)–(c) in detail. From Fig. 4(a), the peaks in the region of 964.00–924.00 eV are clearly observed and attributed to the Cu 2p peaks, suggesting the existence of Cu species on the surface of α-Bi_2O_3 samples. The weight ratio of Cu to α-Bi_2O_3 is 2% according to our measurement, which is higher than the designed amount of 0.4%. This error will be explained in detail in the following. In the CuO_x/α-Bi_2O_3 samples, the CuO_x was deposited on the surface of α-Bi_2O_3 microrods. XPS is known as a surface analysis method and it can only analyze the elements under the surfaces of the materials with the depth of nanometers. Since the shapes of α-Bi_2O_3 are the microrods with dozens of micrometers length and 1–2 μm diameters [Fig. 3(A) and (B)], this results in that the XPS can only explore the Cu on the surfaces and a small part of α-Bi_2O_3. Therefore, the tested Cu weight ratio should be higher than the designed amount in the surface layers which XPS can analyze. From Fig. 4(b), the two peaks with the binding energies of 164.20 and 158.90 eV are ascribed as the Bi

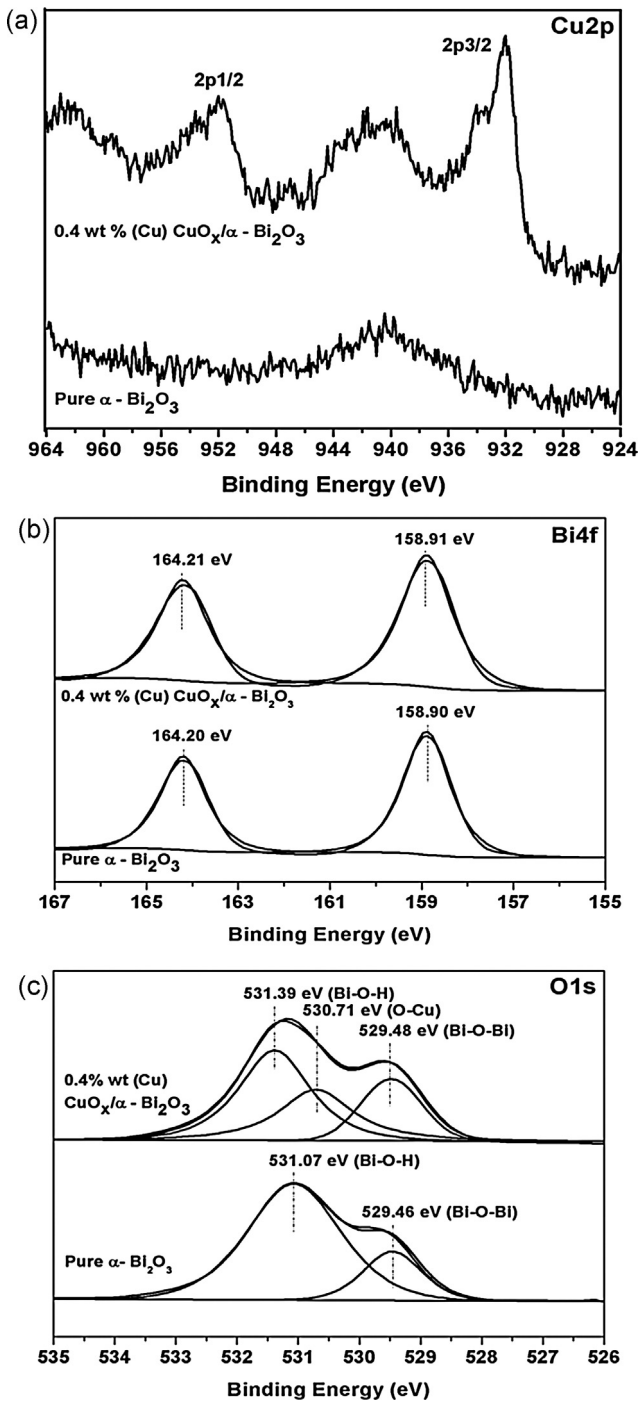

Fig. 4. (a) High-resolution XPS spectra of Cu 2p species in pure α-Bi_2O_3 and CuO_x/α-Bi_2O_3; (b) high-resolution XPS spectra of Bi 4f species in pure α-Bi_2O_3 and CuO_x/α-Bi_2O_3; (c) high-resolution XPS spectra of O 1s species in pure α-Bi_2O_3 and CuO_x/α-Bi_2O_3.

$4f_{5/2}$ and Bi $4f_{7/2}$ peaks, and they are the characteristic peaks of Bi^{3+} in α-Bi_2O_3 [29]. After CuO_x was modified, these two peaks have slight positive shifts to higher energies of 164.21 and 158.91 eV, correspondingly. These shifts may be caused by the modification of CuO_x on the surface of α-Bi_2O_3. From Fig. 4(c), the two peaks of O1s located at 531.07 eV and 529.46 eV are ascribed to the surface oxygen (Bi—O—H) and the lattice oxygen (Bi—O—Bi). Similar to the peaks of Bi 4f, the two peaks of O 1s also have slight positive shifts to higher energies of 531.39 and 529.48 eV. In addition, the new peak at 530.71 eV after CuO_x modification can be assigned to the lattice CuO oxygen. The spectra of Fig. 4(a)–(c) indicate the existence of CuO species on the surface of α-Bi_2O_3, as well as the interaction between them.

Based on the experimental results above, the states of the CuO_x are suggested to be the coexistence of Cu(II) clusters and CuO.

3.2. Photocatalytic performances

To study the effects of the CuO_x for the photocatalytic activity enhancement of α-Bi_2O_3, RhB aqueous solutions were degraded for 3 h under visible light irradiation ($\lambda \geq 420$ nm). The self-degradation experiment of RhB aqueous solution was also carried out in the same manner for comparison. After 3 h irradiation, the RhB aqueous solutions were degraded much more over CuO_x/α-Bi_2O_3 samples than over pure α-Bi_2O_3, except the sample with the Cu weight ratio of 0.8% (Fig. 5a). Meanwhile, much less RhB degradation was observed in the absence of any catalysts. According to the results, the optimum weight ratio of Cu was determined to be 0.4%, and the sample with this Cu weight ratio was chosen as the main research object in all of the following researches. The improvement of the RhB degradation can partly confirm the important effect of the CuO_x in the photocatalytic reactions. As for the less degradation of RhB over CuO_x/α-Bi_2O_3 sample with the Cu weight ratio of 0.8%, it is because that the excessive CuO_x covers the surface of α-Bi_2O_3 and diminishes the light absorption of α-Bi_2O_3. In addition, the degradation of the MO aqueous solutions, as shown in Fig. 5(b), further confirmed the improved photocatalytic activity of CuO_x/α-Bi_2O_3. In these experiments, almost 70% of MO was degraded over CuO_x/α-Bi_2O_3 after 4.5 h visible light irradiation ($\lambda \geq 420$ nm), which is more than three times as that over pure α-Bi_2O_3 (20%).

As we know, the dye-sensitized photooxidation process often occurs between dye-molecular and some semiconductors such as TiO_2 [42] and $SrTiO_3$ [43]. RhB aqueous solutions, with a strong absorbance at the wavelength from 450 nm to 600 nm, were also degraded under the irradiation of four 3 W monochromatic lights ($\lambda = 420$ nm), in order to rule out the disturbance of the dye-sensitization effect. The results in Fig. 5(c) show that CuO_x/α-Bi_2O_3 sample degraded much more (~70%) RhB than pure α-Bi_2O_3 sample (~6%) did, while no self-degradation of RhB occured under the same condition. In order to give a further confirmation of the non-dye-sensitization effect, 2,4-DCP aqueous solutions which have no visible light absorbance, were also degraded under the visible light irradiation ($\lambda \geq 420$ nm). Similar results were observed in these experiments, as shown in Fig. 5(d). After 7 h visible light irradiation, nearly 90% and 45% 2,4-DCP were degraded over CuO_x/α-Bi_2O_3 and pure α-Bi_2O_3 samples, respectively. At the same time, almost 80% and 35% total organic carbon (TOC) were removed respectively in the aqueous suspensions of CuO_x/α-Bi_2O_3 and pure α-Bi_2O_3 with 14 h visible light irradiation. According to our previous reports [16], both the concentration of 2,4-DCP and TOC in the aqueous solution have no significant decrease in the absence of any catalysts, in the same experimental condition. The results in Fig. 5(c) and (d) well confirmed that the photocatalytic activity enhancement of CuO_x/α-Bi_2O_3 is not induced by the dye-sensitization effect.

We also evaluated the photocatalytic activities of both pure α-Bi_2O_3 and CuO_x/α-Bi_2O_3 samples in the gas phase, and IPA was chosen as the degraded target molecular. Encouragingly, the CuO_x/α-Bi_2O_3 sample still exhibits much higher photocatalytic activity than pure α-Bi_2O_3 sample. Fig. 5(e) illustrates the production of acetone, which is the one-hole oxidation product of IPA, over pure α-Bi_2O_3 (~335 ppm) and CuO_x/α-Bi_2O_3 (~1200 ppm) samples under visible light irradiation for 8 h. In order to avoid the single-handed effect of CuO_x, we also carried out the same degradation

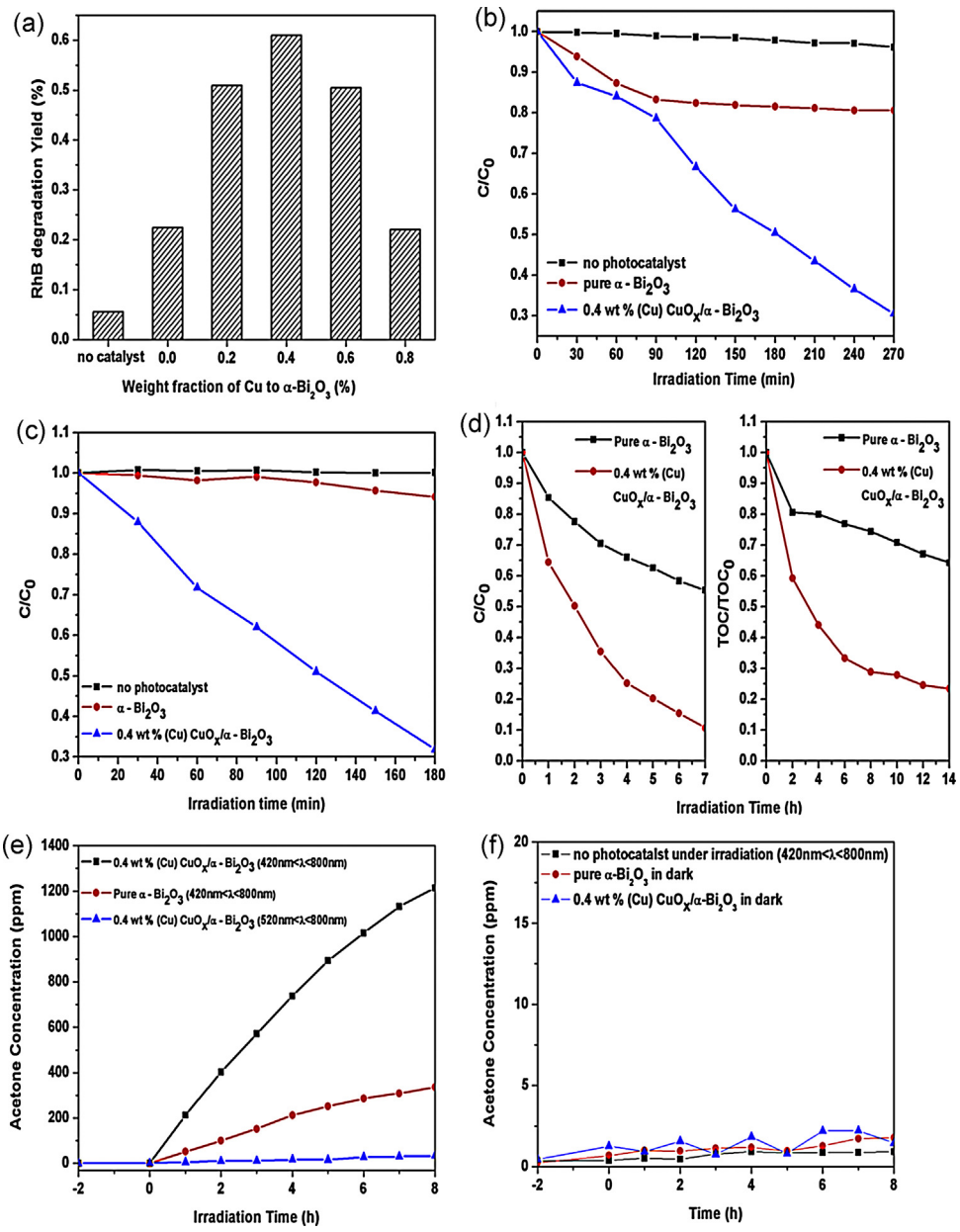

Fig. 5. (a) Photocatalytic degradations of RhB over pure α-Bi_2O_3 and CuO_x/α-Bi_2O_3 with different Cu weight ratios under visible light irradiation ($\lambda \geq 420$ nm) in 3 h; (b) photocatalytic degradations of MO over pure α-Bi_2O_3 and CuO_x/α-Bi_2O_3 under visible light irradiation ($\lambda \geq 420$ nm); (c) photocatalytic degradations of RhB over pure α-Bi_2O_3 and CuO_x/α-Bi_2O_3 under irradiation of monochromatic light ($\lambda = 420$ nm); (d, left), photocatalytic degradations of 2,4-dichorophenol (2,4-DCP) over pure α-Bi_2O_3 and CuO_x/α-Bi_2O_3 under visible light irradiation ($\lambda \geq 420$ nm); (d, right) TOC removal rates of 2,4-DCP aqueous suspensions of different photocatalysts under visible light irradiation ($\lambda \geq 420$ nm); (e) photocatalytic degradations of gaseous IPA over pure α-Bi_2O_3 and CuO_x/α-Bi_2O_3 under visible light irradiation; (f) control experiments of gaseous IPA degradation.

experiments over CuO_x/α-Bi_2O_3 samples under the irradiation of visible light with the wavelength of 520 nm $\leq \lambda \leq$ 800 nm, although its amount is so minute. Just as we expected, little acetone was produced under these conditions. For comparison, some control experiments were also carried out synchronously. From Fig. 5(f), acetone produced over either pure α-Bi_2O_3 or CuO_x/α-Bi_2O_3 sample in the dark, can totally be neglected. Furthermore, the acetone produced from IPA under visible light irradiation in the absence of any catalysts can also be neglected.

All of the results in Fig. 5 convincingly demonstrated that the CuO_x modification is a very effective way to improve the photocatalytic activity of α-Bi_2O_3, for both the degradations of dye-organic contaminants and non-dye-organic contaminants, both in the aqueous solution and gas phase.

3.3. The role of CuO_x

According to the previous reports [30,31,34], Cu(II) is considered as the main effective species for the photocatalytic activity improvement of the semiconductors (TiO_2, WO_3), and acts via an interfacial charge transfer (IFCT) process. Considering the coexistence of Cu(II) clusters and CuO in our system, the similar effect is speculated to describe the role of CuO_x. We called it as CuO_x-assistant electron transfer process (CuO_x-AETP), which involves in two electron excitation paths and a Cu cycle of different valence states. The details are illustrated in Scheme 1. For CuO_x/α-Bi_2O_3, the electrons on the valence band are excited by two paths: path I, the electrons are excited to the conduction band, and then transfer to CuO; path II, the electrons are directly excited to Cu(II) clusters

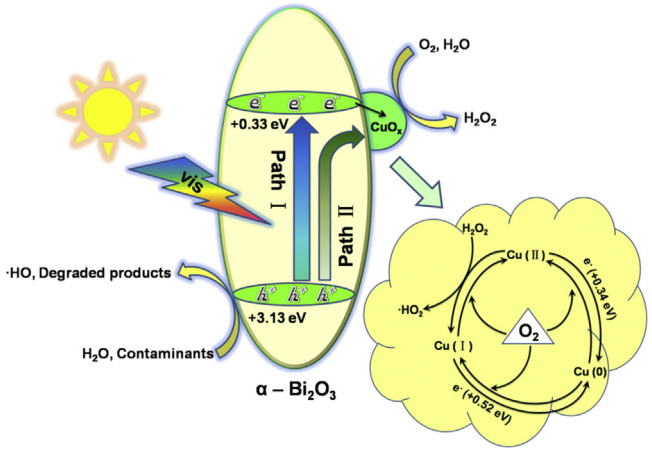

Scheme 1. Schematic illustration of the CuO_x-AETP.

via an interfacial charge transfer (IFCT) process, and this process is proved by the UV–vis absorption in the wavelength of 450–520 nm in Fig. 2. And then, the excited electrons will be consumed constantly by Cu(II) species via a Cu cycle of different valence states. As a result, the valence holes' lifetime of α-Bi_2O_3 is prolonged consumedly, which realizes an efficient separation of the electrons and holes, and enhances the photocatalytic activity of α-Bi_2O_3. The Cu cycle of different valence states is described in detail in Scheme 1, and by the equations [Eqs. (2)–(9)] [44]. Among them, Eq. (3) will be replaced by Eq. (4) because of its more negative electrical potential than the CB level of α-Bi_2O_3 (+0.33 V vs. NHE).

Cu cycle (the consumption of the conduction band electrons):

Consumption of Cu with higher valence states [Cu(II) and Cu(I)]:

$$Cu(II) + e^- \rightarrow Cu(0), \quad \Delta E = +0.34\,eV \tag{2}$$

$$Cu(II) + e^- \rightarrow Cu(I), \quad \Delta E = +0.15\,eV \tag{3}$$

$$Cu(II) + H_2O_2 \rightarrow Cu(I) + {}^{\bullet}HO_2 + H^+ \tag{4}$$

$$Cu(I) + e^- \rightarrow Cu(0), \quad \Delta E = +0.52\,eV \tag{5}$$

Regeneration of Cu with higher valence states [Cu(II) and Cu(I)]:

$$Cu(0) + O_2 + 2H_2O \rightarrow Cu(II) + 2H_2O_2 \tag{6}$$

$$2Cu(0) + O_2 + 2H_2O \rightarrow 2Cu(I) + 2H_2O_2 \tag{7}$$

$$Cu(I) + O_2 + H_2O \rightarrow Cu(II) + H_2O_2 \tag{8}$$

$$Cu(I) + H_2O_2 \rightarrow Cu(II) + OH^- + {}^{\bullet}OH \tag{9}$$

During this process, some radicals such as •OH and $^{\bullet}HO_2$, highly active for decomposing the contaminants, are also generated. The total reaction processes are described as follows:

Total redox reactions:

Reductions:

$$2e_{CB}^- + O_2 + 2H_2O \rightarrow 2H_2O_2 \tag{10}$$

Oxidations:

$$h_{VB}^+ + H_2O(or OH^-) \rightarrow {}^{\bullet}OH \tag{11}$$

$$h_{VB}^+ + contaminants \rightarrow degradedproducts \tag{12}$$

$$^{\bullet}OH + contaminants \rightarrow degradedproducts \tag{13}$$

$$^{\bullet}OH_2 + contaminants \rightarrow degradedproducts \tag{14}$$

In this system, Cu with (0), (I), and (II) valence states are all-referred and act important effects during the CuO_x-AETP. We will have a detailed demonstration in the following context about this process.

3.4. Study of the photocatalytic mechanisms

To prove the important role of CuO_x in the α-Bi_2O_3's photocatalytic activity enhancement, the formations of hydroxyl radicals (•OH) and hydrogen peroxide (H_2O_2) over the two samples, were measured in aqueous suspensions under visible light irradiation (λ = 420 nm). Furthermore, the ESR and XPS were also used to study the valence states change of Cu before and after the photocatalysis.

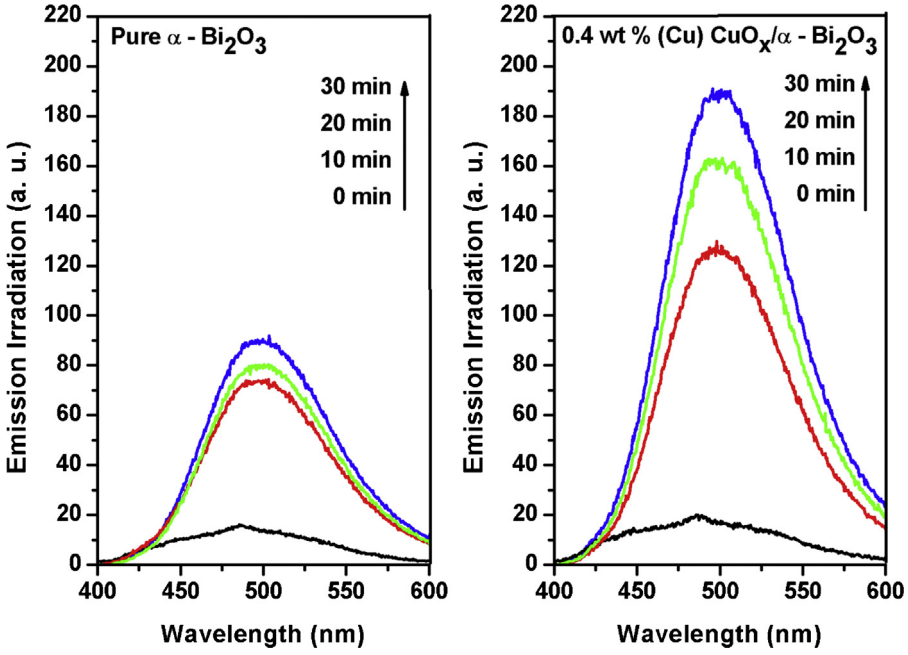

Fig. 6. Fluorescence emission intensities of coumarin–OH adduct (7-hydroxycoumarin) produced in the visible light irradiated suspensions of pure α-Bi_2O_3 and CuO_x/α-Bi_2O_3 in the presence of Fe^{3+} ions.

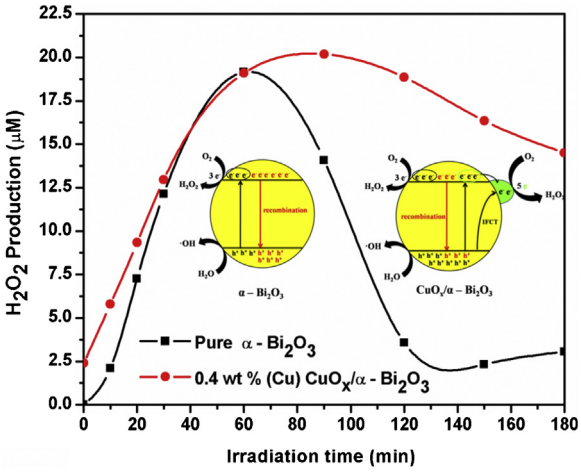

Fig. 7. In situ photogenerated H_2O_2 in the visible light (λ = 420 nm) irradiated suspension of pure α-Bi_2O_3 and CuO_x/α-Bi_2O_3 in the presence of methanol as an electron donor.

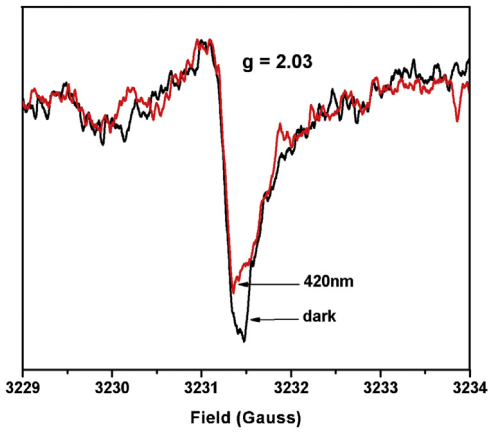

Fig. 8. ESR signals of Cu(II) in CuO_x/α-Bi_2O_3 before and after visible light irradiation (λ ≥ 420 nm).

3.4.1. Analysis of photogenerated •OH

Hydroxyl radicals (•OH) are always considered to be the most important oxidative species in photocatalytic reactions. In our systems, the •OH is produced not only by the oxidation path [Eq. (15)], but also by the reduction path [Eqs. (16) and (17)].

$$h_{VB}^{+} + H_2O(\text{or}OH^{-}) \rightarrow {}^{\bullet}OH \quad (15)$$

$$2e_{CB}^{-} + O_2 + 2H_2O \rightarrow 2H_2O_2 \quad (16)$$

$$H_2O_2 + e_{CB}^{-} \rightarrow OH^{-} + {}^{\bullet}OH \quad (17)$$

In the presence of Fe^{3+}, the reaction of Eq. (16) will be taken place easier by the reduction of Fe^{3+}, which inhibits the two-electron reduction process of O_2 [Eq. (16)], because of a higher redox potential of Fe^{3+}/Fe^{2+} (+0.771 V vs. NHE) than O_2/H_2O_2 (+0.695 V vs. NHE). As a result, the photogenerated •OH will be only produced on the valence band by oxidation path [Eq. (15)]. The fluorescence emission intensities of the coumarin–OH adduct (7-HC) produced in the visible light irradiated aqueous suspensions with pure α-Bi_2O_3 and CuO_x/α-Bi_2O_3 samples, are respectively displayed in Fig. 6. The fluorescence spectra suggest the production of •OH by the formation of 7-HC. From this figure, •OH produced by the two samples are both observed, and the CuO_x/α-Bi_2O_3 produces about twice more than pure α-Bi_2O_3 in 30 min.

3.4.2. Analysis of photogenerated H_2O_2

Hydrogen peroxide (H_2O_2) is considered to be the main product of O_2 reduction by the conduction band electrons via a two-electron process, in α-Bi_2O_3 system [Eq. (16)]. So, the productions of H_2O_2 over pure α-Bi_2O_3 and CuO_x/α-Bi_2O_3 are also important indicators of efficiency photocatalytic performances. In this experiment, H_2O_2 is only produced by the two-electron process [Eq. (16)] due to the presence of methanol, which is a good hole trap. As presented in Fig. 7, the concentrations of H_2O_2 produced by both α-Bi_2O_3 and CuO_x/α-Bi_2O_3 increase firstly and then decrease with the similar trend under 180 min irradiation by visible light. The uptrend of the curves naturally comes from the increases of H_2O_2 with the prolongation of the irradiation time; and the downtrend of the curves may come from the decomposition of H_2O_2 by Eq. (17), according to the literature [45]. We also note that the generation of H_2O_2 is almost the same over the two samples at the first 60 min. After 60 min reaction, the decrease of the H_2O_2 generated over CuO_x/α-Bi_2O_3 is much slower than over α-Bi_2O_3. This result can be explained as follows: In the α-Bi_2O_3 system, the electrons on the valence band of α-Bi_2O_3 are excited into the conduction band, and some of them react with the adsorbed oxygen to form H_2O_2, while the others recombined with the holes. However, it is more complex in the CuO_x/α-Bi_2O_3 system. On one hand, the electrons on the valence band of α-Bi_2O_3 are excited directly into the Cu(II) clusters via an IFCT process. On the other hand, the electrons are excited into the conduction band. After that, some of the excited electrons transfer to the CuO clusters; some of them go to reduce the adsorbed oxygen into H_2O_2; the left electrons recombined with the holes. When the first process is faster than the second, partial electrons will stay in the Cu clusters and could not react with the adsorbed oxygen to form H_2O_2 immediately. Therefore, the generation of H_2O_2 by CuO_x/α-Bi_2O_3 should not be much higher than pure α-Bi_2O_3 at the beginning. When the Cu(II) was almost reduced, the generation of the H_2O_2 by CuO_x/α-Bi_2O_3 starts to become more than pure α-Bi_2O_3. As a result, the decrease of the H_2O_2 generated over CuO_x/α-Bi_2O_3 is much slower than over α-Bi_2O_3, when the decompositions of the H_2O_2 are present at the same time. In the earlier reports, we have a similar discussion [16]. The slower H_2O_2 decomposition by CuO_x/α-Bi_2O_3 indicates that it is a constant and stable photocatalyst.

All of the results above forcefully proved that CuO_x modification significantly promotes the separation of α-Bi_2O_3's electrons and holes.

3.4.3. ESR and XPS experiments

According to the earlier literature [31], the consumption of Cu(II) can be proved by the ESR measurements in the absence of O_2. To avoid the regeneration of Cu(II) by the hole oxidation, methanol was added not only as the solvent, but also as a hole trap. As shown in Fig. 8, a signal was clearly observed in the region of 3229–3234 G, being attributed to the ESR signal of Cu(II). After 10 min irradiation of the visible light with the wavelength of λ ≥ 420 nm, there is a significant decrease of the Cu(II). That is because that the absence of O_2 and the presence of the methanol inhibit the regeneration of Cu(II) after it is reduced by the photoexcited electrons. The decrease of Cu(II) indicates that the Cu(II) was really reduced to lower valence states during the visible light irradiation.

The Cu species in the CuO_x clusters were specified by the high-resolution XPS of Cu 2p. The high-resolution XPS spectrum of the Cu 2p peaks in the region of 964.00–924.00 eV was studied in detail and presented in Fig. 9. The peaks in the regions of 958.00–949.00 eV and 949.00–925.00 eV are attributed to the Cu $2p_{1/2}$ and Cu $2p_{3/2}$, respectively [46]. As we expected, the peaks of Cu(II) can be clearly observed from Fig. 9, as well as its satellite peaks. However, we can also see the peaks of Cu in another type, i.e. Cu(0) or Cu(I), in this spectrum. Because of nearly the same peaks of binding energies and

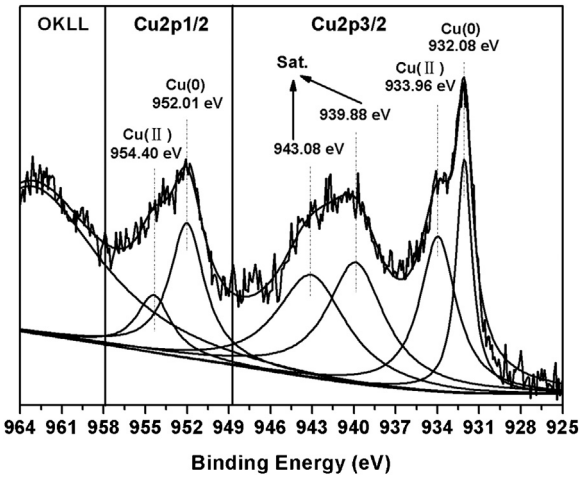

Fig. 9. High-resolution XPS spectrum of Cu 2p in CuO_x/α-Bi_2O_3.

shapes for Cu(0) and Cu(I) [47], it is difficult to distinguish them. Considering the instability of Cu(I), we attribute it to Cu(0). At last, the existence of Cu(0) in CuO_x/α-Bi_2O_3 sample is another important reason that we call it as CuO_x/α-Bi_2O_3 but not CuO/α-Bi_2O_3 or Cu(II)/α-Bi_2O_3. In addition, the amounts of Cu(II) in CuO_x/α-Bi_2O_3 samples, before and after the photocatalysis were also measured by the high-resolution XPS spectra of Cu 2p (Fig. S1). The ratio of Cu(II) is decided to be about 41.42% in the CuO_x clusters before photocatalysis, while it is about 40.78% after the photocatalysis. There is almost no decrease of Cu(II) during the photocatalysis process. It clearly demonstrates the recovery of Cu(II) during the photocatalysis process at the atmosphere.

4. Conclusions

In summary, all the CuO_x modified α-Bi_2O_3 samples show better photocatalytic activity for the degradation of RhB (except the sample with the weight ratio of 0.8%), especially the sample with the Cu weight ratio of 0.4%. It exhibits excellent photocatalytic activities for the degradation of RhB, MO, 2,4-DCP, and the gaseous IPA, showing a good universality. The CuO_x modification is proposed because of the coexistence of Cu(II) clusters, CuO and Cu(0), as well as their important contributions [including Cu(I)] to the photocatalytic activity enhancement of α-Bi_2O_3. The photocatalytic performances of pure α-Bi_2O_3 and CuO_x/α-Bi_2O_3 samples were also studied by measuring the photogenerated •OH and H_2O_2 over them under visible light irradiation. The results indicate the improved separation of the photogenerated electrons and holes by CuO_x modification on the surface of α-Bi_2O_3. Based on the experiments, a CuO_x-assistant electron transfer process (CuO_x-AETP) is proposed and demonstrated. This process involves in two electron excitation paths and a Cu cycle of different valence states. The electrons on the valence band of α-Bi_2O_3 can be excited through two paths: path I, naturally, the electrons are excited to the conduction band of α-Bi_2O_3, and transfer to CuO_x; path II, the electrons are directly excited to the Cu(II) clusters via an interfacial charge transfer (IFCT) process. Then, the excited electrons are consumed consistently by a Cu cycle of different valence states [Cu(II), Cu(I) and Cu(0)]. The consumption and recovery of Cu(II) are demonstrated by the ESR and XPS measurements, respectively. This paper comprehensively researches the excellent photocatalytic activity of CuO_x/α-Bi_2O_3, and systematically elaborates its photocatalytic mechanism on the basis of large amounts of the experimental evidences.

Acknowledgements

This work received financial support from the World Premier International Research Center Initiative (WPI Initiative) on Materials Nanoarchitectonics (MANA), MEXT, Japan, National Natural Science Foundation of China (21273281), National Basic Research Program of China (973Program, No. 2013CB632405), the Fundamental Research Funds for the Central Universities and the Research Funds of Renmin University of China (13XNH121), and the National Scholarship Fund.

Appendix A. Supplementary data

Supplementary data associated with this article can be found, in the online version, at http://dx.doi.org/10.1016/j.apcatb.2014.07.058.

References

[1] A. Fujishima, K. Honda, Nature 238 (1972) 37–38.
[2] K. Cheng, W. Sun, H.-Y. Jiang, J. Liu, J. Lin, J. Phys. Chem. C 117 (2013) 14600–14607.
[3] J. Yu, Q. Li, S. Liu, M. Jaroniec, Chem. Eur. J. 19 (2013) 2433–2441.
[4] X. Zhang, U. Veikko, J. Mao, P. Cai, T. Peng, Chem. Eur. J. 18 (2012) 12103–12111.
[5] Z. Zheng, J. Zhao, Y. Yuan, H. Liu, D. Yang, S. Sarina, H. Zhang, E.R. Waclawika, H. Zhu, Chem. Eur. J. 19 (2013) 5731–5741.
[6] M.R. Hoffmann, S.T. Martin, W. Choi, D.W. Bahnemann, Chem. Rev. 95 (1995) 69–96.
[7] G. Begum, J. Manna, R.K. Rana, Chem. Eur. J. 18 (2012) 6847–6853.
[8] Y. Liu, J. Shi, Q. Peng, Y. Li, Chem. Eur. J. 19 (2013) 4319–4326.
[9] L. Wu, J. Xing, Y. Hou, F.Y. Xiao, Z. Li, H.G. Yang, Chem. Eur. J. 19 (2013) 8393–8396.
[10] I. Paramasivam, Y.C. Nah, C. Das, N.K. Shrestha, P. Schmuki, Chem. Eur. J. 16 (2010) 8993–8997.
[11] G. Xi, Y. Yan, Q. Ma, J. Li, H. Yang, X. Lu, C. Wang, Chem. Eur. J. 18 (2012) 13949–13953.
[12] M. Shang, W. Wang, L. Zhang, S. Sun, L. Wang, L. Zhou, J. Phys. Chem. C 113 (2009) 14727–14731.
[13] R. Shi, G. Huang, J. Lin, Y. Zhu, J. Phys. Chem. C 113 (2009) 19633–19638.
[14] K. Brezesinski, R. Ostermann, P. Hartmann, J. Perlich, T. Brezesinski, Chem. Mater. 22 (2010) 3079–3085.
[15] A. Hameed, T. Montini, V. Gombac, P. Fornasiero, J. Am. Chem. Soc. 130 (2008) 9658–9659.
[16] H.-Y. Jiang, K. Cheng, J. Lin, Phys. Chem. Chem. Phys. 14 (2012) 12114–12121.
[17] H.-Y. Jiang, J. Liu, K. Cheng, W. Sun, J. Lin, J. Phys. Chem. C 117 (2013) 20029–20036.
[18] F. Qin, G. Li, R. Wang, J. Wu, H. Sun, R. Chen, Chem. Eur. J. 18 (2012) 16491–16497.
[19] L. Zhou, W. Wang, H. Xu, S. Sun, M. Shang, Chem. Eur. J. 15 (2009) 1776–1782.
[20] J. Hu, H. Li, C. Huang, M. Liu, X. Qiu, Appl. Catal. B: Environ. 142–143 (2013) 598–603.
[21] Z. Kelly, F. Ojebuoboh, JOM 54 (2002) 42–45.
[22] F.G. Lin, Y. Takao, Y. Shimizu, M. Egashira, J. Am. Ceram. Soc. 78 (1995) 2301–2306.
[23] D. Liu, Y. Liu, S.Q. Huang, X. Yao, J. Am. Ceram. Soc. 76 (1993) 2129–2132.
[24] A. Hameed, V. Gombac, T. Montini, M. Graziani, P. Fornasiero, Chem. Phys. Lett. 472 (2009) 212–216.
[25] Y. Xu, M.A. Schoonen, Am. Mineral. 85 (2000) 543–556.
[26] L. Li, Y.W. Yang, G.H. Li, L.D. Zhang, Small 2 (2006) 548–553.
[27] C. Wang, C. Shao, L. Wang, L. Zhang, X. Li, Y. Liu, J. Colloid Interface Sci. 333 (2009) 242–248.
[28] M. Ge, Y. Li, L. Liu, Z. Zhou, W. Chen, J. Phys. Chem. C 115 (2011) 5220–5225.
[29] Z. Bian, J. Zhu, S. Wang, Y. Cao, X. Qian, H. Li, J. Phys. Chem. C 112 (2008) 6258–6262.
[30] G. Li, N.M. Dimitrijevic, L. Chen, T. Rajh, K.A. Grey, J. Phys. Chem. C 112 (2008) 19040–19044.
[31] H. Irie, K. Kamiya, T. Shibanuma, S. Miura, D.A. Tryk, T. Yokoyama, K. Hashimoto, J. Phys. Chem. C 113 (2009) 10761–10766.
[32] X. Qiu, M. Miyauchi, K. Sunada, M. Minoshima, M. Liu, D. Li, Y. Shimodaira, Y. Hosogi, Y. Kuroda, K. Hashimoto, ACS Nano 6 (2012) 1609–1618.
[33] Q. Jin, M. Fujishima, M. Nolan, H. Tada, A. Iwaszuk, J. Phys. Chem. C117 (2013) 23848–23857.
[34] T. Arai, M. Yanagida, Y. Konishi, A. Ikura, Y. Iwasaki, H. Sugihara, K. Sayama, Appl. Catal. B: Environ. 84 (2008) 42–47.
[35] X. Qiu, M. Miyauchi, H. Ye, H. Irie, K. Hashimoto, J. Am. Chem. Soc. 132 (2010) 15259–15267.
[36] K.-I. Ishibashi, A. Fujishima, T. Watanabe, K. Hashimoto, Electrochem. Commun. 2 (2000) 207–210.
[37] H. Bader, V. Sturzenegger, J. Hoigne, Water Res. 22 (1988) 1109–1115.
[38] M. Drache, P. Roussel, J.-P. Wignacourt, Chem. Rev. 107 (2007) 80–96.

[39] S. Anandan, G.-J. Lee, P.-K. Chen, C. Fan, J.J. Wu, Ind. Eng. Chem. Res. 49 (2010) 9729–9737.
[40] Y. Liu, Y. Chu, Y. Zhuo, M. Li, L. Li, L. Dong, Cryst. Growth Des. 7 (2007) 467–470.
[41] X. Zhang, G. Wang, X. Liu, J. Wu, M. Li, J. Gu, H. Liu, B. Fang, J. Phys. Chem. C 112 (2008) 16845–16849.
[42] Y. Cho, W. Choi, C.-H. Lee, T. Hyeon, H.-I. Lee, Environ. Sci. Technol. 35 (2001) 966–970.
[43] S. Yang, H. Kou, J. Wang, H. Xue, H. Han, J. Phys. Chem. C 114 (2010) 4245–4249.
[44] Z. Wang, A. Von Dem Bussche, P.K. Kabadi, A.B. Kane, R.H. Hurt, ACS Nano 7 (2013) 8715–8727.
[45] T. Wu, G. Liu, J. Zhao, H. Hidaka, N. Serpone, J. Phys. Chem. B 103 (1999) 4862–4867.
[46] Y.H. Kim, D.K. Lee, H.G. Cha, C.W. Kim, Y.C. Kang, Y.S. Kang, J. Phys. Chem. B 110 (2006) 24923–24928.
[47] J. Espinos, J. Morales, A. Barranco, A. Caballero, J. Holgado, A. Gonzalez-Elipe, J. Phys. Chem. B 106 (2002) 6921–6929.